Locomotive Control of a Wearable Lower Exoskeleton for Walking Enhancement

K. H. LOW
XIAOPENG LIU
School of Mechanical and Aerospace Engineering, Nanyang Technological University, Singapore 639798, Republic of Singapore (mkhlow@ntu.edu.sg)

C. H. GOH
HAOYONG YU
DSO National Laboratories, 20 Science Park Drive, Singapore 118230, Republic of Singapore

(Received 20 January 2006; accepted 15 May 2006)

Abstract: This article presents a wearable lower extremity exoskeleton (LEE) designed to augment the ability of a human to walk while carrying payloads. The ultimate goal of the current research is to design and control a wearable power-assisted system that integrates a human's intellect as the control command. The system in this work consists of an inner exoskeleton and an outer exoskeleton. The inner system measures the movements of the human and controls the outer system, which follows the human movements and supports the payload. A special foot-unit was designed to measure the zero moment points (ZMPs) of the human and the exoskeleton simultaneously. Using the measured human ZMP as the reference, the exoskeleton's ZMP is controlled by trunk compensation to achieve stable walking. A COTS program, xPC Target, together with toolboxes from MATLAB, were used as a real-time operating system and integrated development environment, and real-time locomotion control of the exoskeleton was successfully implemented in this environment. Finally, some walking experimental results, by virtue of the ZMP control for the inner and outer exoskeletons, show that the stable walking can be achieved.

Keywords: Lower extremity exoskeleton, wearable power-assisted system, ZMP control, locomotion control, walking test

1. INTRODUCTION

Even though research on humanoid robots has been conducted for many years, there are currently no robots able to preserve the same quality of performance as humans in performing tasks under a wide range of fuzzy conditions. Compared to a human's naturally developed algorithms, which contain complex and highly specialized control methods, the artificial control algorithms for robots lack flexibility. On the other hand, robots can easily perform certain tasks that humans are unable to match because of their physical limitations, such as maneuvering heavy objects. It seems therefore that combining the human and the robot into

Journal of Vibration and Control, **12(12):** 1311–1336, 2006 DOI: 10.1177/1077546306070616

Figures 4, 5, 7, 10, 11, 13–15, 17–20, 22–25 appear in color online: http://jvc.sagepub.com

one integrated system under the control of the human may lead to a solution able to benefit from the advantages offered by each subsystem. Exoskeletons are systems based on this principle.

Exoskeletons for human performance enhancement are controlled wearable devices intended to increase the speed, strength, and endurance of the operator. The human provides control signals for the exoskeleton, while the actuators of the exoskeleton provide most of the power necessary for performing the task. The human applies a scaled-down force compared to the load carried by the exoskeleton.

Lower extremity exoskeletons can be categorized into two types based on the intended application; walking aids for people with gait disorders or the elderly, and power augmentation systems to enhance the payload-carrying ability of normal persons.

People with gait disorders and elderly people who are unable to walk without assistance may lose muscular strength in their legs and become bedridden. They can only move around in a wheelchair or using a wheeled walker. Unfortunately, barriers such as bumps and steps restrict the area that these people have access to. However, a the lower exoskeleton could be used to enhance their muscular strength and enable them walk better. One of the most well-known attempts is the Hybrid Assistive Leg (HAL) developed by Sankai et al. (Kasaoka and Sankai, 2001; Kawamoto and Sankai, 2002). HAL can provide assistive torques at the user's hip and knee joints, based on the user's intention as determined using EMG (electromyogram) signals, using these signals as the primary command signal together with angular sensors and floor reaction sensors. With the motors, measurement system, computer, wireless LAN (local area network), and power supply built in the backpack, HAL works as a completely wearable system.

The second type of exoskeleton is proposed to help those who need to travel long distances on foot with heavy loads, such as infantry soldiers. Because the structure of the exoskeleton can be much stronger than human legs, it can carry heavy loads that a person would be unable to manage. With the help of the exoskeleton, the user can carry higher loads and walk longer before getting tired.

The lower back is the area most vulnerable to injury when carrying heavy loads, due to the compressive force applied to lower vertebrae. A group at Hokkaido University has developed a wearable power assistive device for a human's lower back (Kawai et al., 2004; Naruse et al., 2003a,b). The group's power device assists flexion and extension of the lower back, reduces compressive force, and generates negative force to assist lifting. In the year 2000, Kazerooni and his research team in the Berkeley Robotics Laboratory began to develop the Berkeley lower extremity exoskeleton (BLEEX, http://bleex.me.berkeley.edu/bleex.htm), which is funded by the US Defense Advanced Research Projects Agency (DARPA). Three years later, the first fully functional prototype experimental exoskeleton was demonstrated. The system is comprised of two powered anthropomorphic legs, a power unit, and a backpack-like frame on which a variety of loads can be mounted. More than 40 sensors, including some embedded within the shoe pads, and hydraulic actuators, form a LAN for the exoskeleton and function much like a human nervous system. The exoskeleton uses a small state of the art hybrid power source, which delivers hydraulic power for locomotion and electrical power for the exoskeleton computer.

In collaboration with Singapore's DSO National Laboratories, a team at the Nanyang Technological University (NTU) has constructed a lower extremity exoskeleton (LEE) system in Singapore (Liu and Low, 2004; Liu et al., 2004; Low et al., 2004). The human

provides control signals to the exoskeleton, while the exoskeleton actuators provide most of the power needed to carry the payload. The system might provide soldiers, fire fighters, disaster relief workers, and other emergency personnel the ability to carry heavy loads such as food, weaponry, rescue equipment, and communications gear with minimal effort over any type of terrain for extended periods of time. In the following sections, the background to, and features of, the LEE are introduced, together with the real time control strategy and the walking experiments. We will first present the features of biped gaits and the dynamics of the exoskeleton. The principle of the control strategy will then be discussed, including locomotion control and control of the ZMP. The implementation of the control strategy on the final prototype is introduced in Section 4, and conclusions and future work are presented in the final section.

2. GAIT DYNAMICS

Biped locomotion has been the focus of research for decades. It is well known that a biped gait can be divided into two phases: The single support phase and the double support phase (Whittle, 1991). In the single support phase, one leg is moving in the air while the other leg is in contact with the ground. In the double support phase, both feet are in contact with the ground. The two support phases take place alternately during walking.

All of the biped mechanism joints are powered and directly controllable, except for the contact area between the foot and the ground. Foot behavior cannot be controlled directly, but is controlled indirectly by ensuring appropriate dynamics of the mechanism above the foot. To account for this, the concept of the zero moment point (ZMP) (Vukobratović and Duvicic, 1969), defined as the point on the ground at which the net moment of the inertial forces and the gravity forces has no horizontal component, has been used. The gait is balanced provided that the ZMP trajectory remains within the support area. In this case, the system dynamics are perfectly balanced by the ground reaction force and the system will not overturn. In the single-support phase, the support polygon is identical to the foot surface. In the double support phase, however, the size of the support polygon is defined by the size of the foot surface and by the distance between them (the convex hull of the two supporting feet). The ZMP concept provides a useful dynamic criterion for the analysis and synthesis of biped locomotion. It can be used to ensure balance during the entire gait cycle and provides a quantitative measure for the unbalanced moment about the support foot and for the robustness (balancing margin) of the dynamic gait equilibrium.

The center of pressure (CoP) (Vukobratović et al., 2001) is also commonly used in biped gait analysis based on force or pressure measurements. The CoP represents the point on the support foot polygon at which the resultant of the distributed foot ground reaction force acts. From their definitions, it is obvious that in the single-support phase, in balanced dynamic gait equilibrium, the ZMP coincides with the CoP. However, in the dynamically unbalanced single-support situation that is characterized by a moment about the CoP that cannot be balanced by the reaction forces on the foot, as shown in Figure 1, the CoP and the ZMP do not coincide. The position of the ZMP outside the support area (determined by the vector $\vec{r}$ in Figure 1) provides useful information for gait balancing. The fact that the ZMP is momentarily on the edge of, or outside, the support polygon indicates the occurrence of an

Figure 1. The ZMP and CoP (from Vukobratović et al., 2001).

unbalanced moment that cannot be compensated for by foot reaction forces. The distance of the ZMP from the foot edge provides a measure of the unbalanced moment (which will tend to rotate the biped around the supporting foot and, possibly, cause a fall).

As depicted in Figure 2, the exoskeleton under consideration is composed of the trunk, pelvis, two shanks, two thighs and two feet. The trunk carries the payload, which can be regarded as a part of the trunk. The vertical Z-axis and horizontal X-axis lie in the sagittal plane, as shown in Figure 2. It can be seen that typical human joint trajectories have a greater motion range in the sagittal plane than in other planes (Marchese et al., 2001) and most movements during walking happen in the sagittal plane. Hence, in the initial design, only the joints rotating around the Y-axis are actuated, and only movements in the sagittal plane are studied.

The dynamical equation that describes the movement of a biped (or exoskeleton) has the following form:

$$M(\vec{q})\ddot{\vec{q}} = f(\vec{q}, \dot{\vec{q}}) + \vec{Q} \tag{1}$$

where $\vec{q} = (q_1, q_2, \ldots, q_7)^T$ is the vector of generalized coordinates (i.e., the joint angles). The matrix function $M(\vec{q})$ takes into account the mass distribution, and the vector function $f(\vec{q}, \dot{\vec{q}})$ describes the effect of both inertial and gravity forces. The elements of the vector $\vec{Q}$ are generalized forces applied to the system, and dots denote time derivatives.

The exoskeleton's structure is a set of rigid bodies connected by revolving joints. Two adjacent links $\{C_i, C_k\}$ connected by a joint at point Z_{ik} are called a kinematic pair. Figure 3 shows a kinematic pair whose joint angle is q_i (i = 1, 2, ... 7), where $\begin{bmatrix} \vec{i}_i & \vec{j}_i & \vec{k}_i \end{bmatrix}$ is the local orthogonal coordinate frame attached to the center of mass of link i, $\vec{e}_i$ is the unit vector of the axes of joint i, and $\vec{r}_{ik}$ is the position vector from point Z_{ik} to the center of mass of link

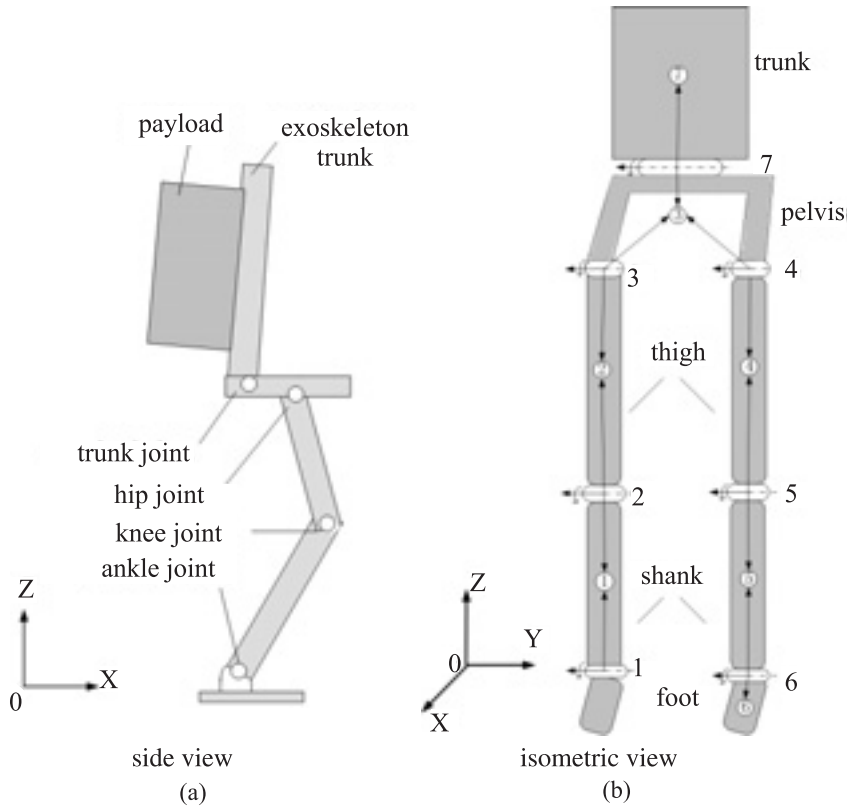

Figure 2. Model of the exoskeleton.

i. The kinematic pairs form kinematic chains. Taking the supporting foot, which is connected to the ground, as C_0, the exoskeleton has two simple chains $\{C_1, C_2, C_3, C_4, C_5, C_6\}$ and $\{C_1, C_2, C_3, C_7\}$, as shown in Figure 2b. Only the first chain is explained here; the second chain can be solved in a similar way.

We set the zero joint coordinates (i.e., $q_i = 0$) to be the home position of all the links. For $R_i^0 = \left[\begin{array}{ccc} \vec{q}_{i1}^0 & \vec{q}_{i2}^0 & \vec{q}_{i3}^0 \end{array} \right]$, which represents the transformation matrix of the i-th link coordinate frame onto the global frame when $q_i = 0$, there exists

$$R_i^0 = \left[\begin{array}{ccc} \vec{e}_i^0 & \vec{a}_i^0 & \vec{e}_i^0 \times \vec{a}_i^0 \end{array} \right] \left[\begin{array}{ccc} \vec{\tilde{e}}_i & \vec{\tilde{a}}_i & \vec{\tilde{e}}_i \times \vec{\tilde{a}}_i \end{array} \right]^T \tag{2}$$

$$\vec{a}_i^0 = \frac{\vec{e}_i^0 \times \left(\vec{r}_{i-1,i}^0 \times \vec{e}_i^0 \right)}{\left| \vec{e}_i^0 \times \left(\vec{r}_{i-1,i}^0 \times \vec{e}_i^0 \right) \right|} \tag{3}$$

$$\vec{\tilde{a}}_i = -\frac{\vec{\tilde{e}}_i \times (\vec{\tilde{r}}_{ii} \times \vec{\tilde{e}}_i)}{\left| \vec{\tilde{e}}_i \times \left(\vec{\tilde{r}}_{ii} \times \vec{\tilde{e}}_i \right) \right|} \tag{4}$$

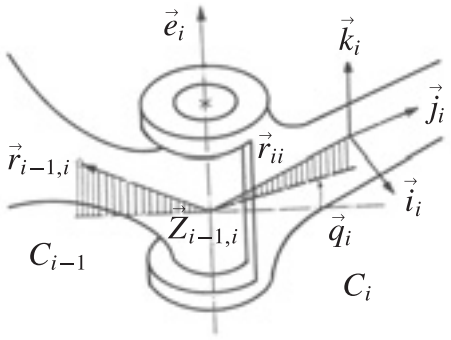

Figure 3. Joint coordinate of a revolving kinematic pair $\{C_{i-1}, C_i\}$.

$$\vec{r}^{\,0}_{i,i+1} = R_i^0 \tilde{\vec{r}}_{i,i+1} \tag{5}$$

$$\vec{e}^{\,0}_{i+1} = R_i^0 \tilde{\vec{e}}_{i+1} \tag{6}$$

where in which $\tilde{(.)}$ represents $(.)$ expressed in the local coordinate frame. By virtue of recursive computation using equations (2) to (6), R_i^0 can be obtained. Next, applying the theorem of finite rotations (Rodrigue's formula) for the revolving joints, one obtains

$$\vec{q}_{ij} = \left[\begin{array}{ccc} \vec{e}_i \times \left(\vec{q}^{\,0}_{ij} \times \vec{e}_i\right) & \vec{e}_i \times \vec{q}^{\,0}_{ij} & \left(\vec{e}_i \cdot \vec{q}^{\,0}_{ij}\right) \vec{e}_i \end{array} \right] \left[\begin{array}{c} \cos q_i \\ \sin q_i \\ 1 \end{array} \right], \quad j = 1, 2, 3. \tag{7}$$

Therefore, the matrix $R_i = \left[\begin{array}{ccc} \vec{q}_{i1} & \vec{q}_{i2} & \vec{q}_{i3} \end{array} \right]$ represents the transformation matrix from the i-th link coordinate system into the global system when $q_i \neq 0$, is determined, where $\vec{e}_{i+1} = R_i \tilde{\vec{e}}_{i+1}$ and $\vec{e}_1$ is known. Hence, the position vectors with respect to the global system are obtained as follows:

$$\begin{aligned} \vec{r}_{ii} &= R_i \tilde{\vec{r}}_{ii} \\ \vec{r}_{i,i+1} &= R_i \tilde{\vec{r}}_{i,i+1}. \end{aligned} \tag{8}$$

Applying the basic theorems of rigid body kinematics, we obtain the following recursive equations:

$$\begin{aligned} \vec{\omega}_i &= \vec{\omega}_{i-1} + \dot{q}_i \vec{e}_i \\ \vec{v}_i &= \vec{v}_{i-1} + \vec{\omega}_{i-1} \times \vec{r}_{i-1,i} + \vec{\omega}_i \times \vec{r}_{ii} \\ \vec{\alpha}_i &= \vec{\alpha}_{i-1} + \dot{q}_i \vec{\omega}_{i-1} \times \vec{e}_i + \ddot{q}_i \vec{e}_i \end{aligned}$$

$$\begin{aligned}\vec{a}_i &= \vec{a}_{i-1} + \vec{\alpha}_{i-1} \times \vec{r}_{i-1,i} + \vec{\omega}_{i-1} \times \left(\vec{\omega}_{i-1} \times \vec{r}_{i-1,i}\right) \\ &+ \vec{\alpha}_i \times \vec{r}_{ii} + \vec{\omega}_i \times (\vec{\omega}_i \times \vec{r}_{ii}) \end{aligned} \tag{9}$$

where $\vec{\omega}_i$, $\vec{v}_i$, $\vec{\alpha}_i$ and $\vec{a}_i$ are the angular velocity, linear velocity of the center of mass, angular acceleration, and linear acceleration of the center of mass of the i-th link, respectively. The inertial force of the center of mass of the i-th link $\vec{F}_i$ and moment of the i-th link $\vec{M}_i$ can then be obtained by using the Newton-Euler equations

$$\begin{aligned}\vec{F}_i &= m_i \vec{a}_i \\ \vec{M}_i &= I_i \vec{\alpha}_i \end{aligned} \tag{10}$$

with

$$\begin{aligned} I_i &= \sum_{l=1}^{3} R_{il} J_{il} \\ R_{il} &= \left[\begin{array}{ccc} q_{il}^1 \vec{q}_{il} & q_{il}^2 \vec{q}_{il} & q_{il}^3 \vec{q}_{il} \end{array} \right] \end{aligned} \tag{11}$$

where m_i is the mass of link i. Note that q_{il}^j (j = 1, 2, 3) denotes the j-th component of vector $\vec{q}_{il}$, and J_{il} is the principal moment of inertia of link i.

3. CONTROL STRATEGY

An important feature of the exoskeleton system, which is also the main difference between an exoskeleton and a bipedal robot, is the participation of a human in the process of control and decision-making. By introducing a human as part of the control system, some tasks that have proven intractable for robots, such as navigation, path planning, obstacle crossing and gait selection, can be undertaken by the pilot instead of the robot's complex artificial controller and vision system. However, two problems remain for the exoskeleton controller to solve: How to transfer the pilot's intention to the exoskeleton and how to keep the exoskeleton stable. Accordingly, the proposed control strategy can be divided into two parts; locomotion control and ZMP control.

3.1. Locomotion Control

During the single support phase, the trajectory of the swinging foot determines gait parameters such as step length, step height, etc. To make sure that the exoskeleton and the wearer can walk together, the trajectory of the exoskeleton's foot swing should trace that of the user in time. To achieve this, a mechanical linkage called an *inner exoskeleton* is attached to the human operator, as shown in Figure 4. Accordingly, the exoskeleton that carries the payloads (and is controlled by the inner exoskeleton) is called the *outer exoskeleton*. The inner exoskeleton is equipped with encoders to capture information about the pilot's joints.

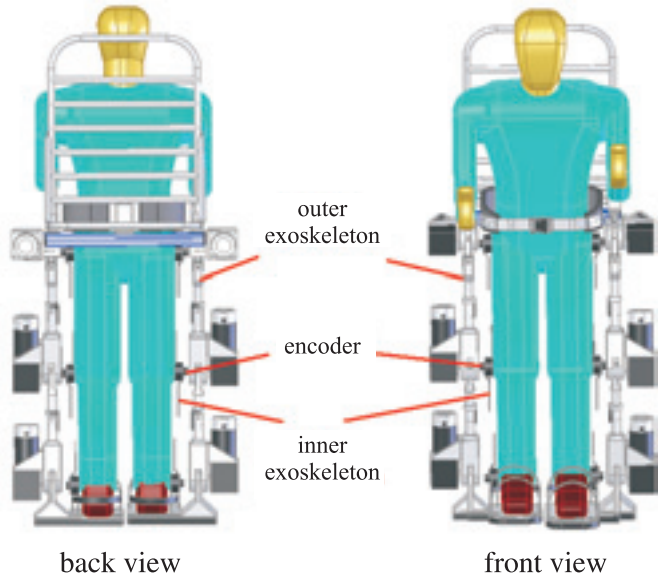

Figure 4. Inner and outer exoskeletons.

3.2. Control of the ZMP

If the ZMP of the exoskeleton is within the support area, that implies that the exoskeleton can remain stable using only the ground reaction force, without applying any force to the user. In other words, the user will not feel any extra burden from the exoskeleton. Hence the purpose of the ZMP control is to make sure the ZMP remains within the support polygon.

From the definition of the ZMP, we have

$$(\vec{M}_G + \vec{M}_F) \cdot \vec{e}_X = 0 \tag{12}$$

$$(\vec{M}_G + \vec{M}_F) \cdot \vec{e}_Y = 0 \tag{13}$$

where $\vec{M}_G$ is the total movement of gravity forces with respect to ZMP, $\vec{M}_F$ is the total moment of inertial forces of all the links with respect to ZMP, and $\vec{e}_X$ and $\vec{e}_Y$ denote unit vectors of the X and Y axes of the absolute coordinate frame. Equation (13) can be further replaced with

$$\sum_{i=1}^{7} \left[(\vec{p}_i - \vec{p}_z) \times \left(G_i + \vec{F}_i \right) + \vec{M}_i \right] . \vec{e}_Y = 0 \tag{14}$$

where $\vec{p}_z$ is the ZMP's coordinates in the global coordinate frame and $\vec{p}_i$ is the position vector of the center of mass of the i-th link,

$$\vec{p}_i = \vec{p}^* + \sum_{j=1}^{i-1} \left(\vec{r}_{jj} - \vec{r}_{j,j+1}\right) + \vec{r}_{ii} \tag{15}$$

where $G_i = m_i g$ is the gravitational force on link i and $\vec{p}^*$ is the position vector of joint 1 with respect to the global coordinate system. Substituting equations (9), (10), (11), and (15) into equation (14), one can obtain

$$\sum_{i=1}^{7} a_i \ddot{q}_i + \sum_{i=1}^{7} \sum_{j=1}^{7} b_{ij} \dot{q}_i \dot{q}_j + \sum_{i=1}^{7} c_i G_i = 0 \tag{16}$$

where the coefficients a_i, b_{ij} and c_i are functions of the generalized coordinates q_i. The trajectories of q_1 to q_6 are determined by the signals measured from the pilot's legs, as mentioned before, while q_7 is determined according to equation (16) to ensure the ZMP remains in the support polygon. However, the actual ZMP may be different from the desired ZMP for all kinds of reasons, such as disturbance from the environment or malfunction of the actuators. A foot-unit that can measure the actual ZMP online was therefore designed.

3.3. Measurement of ZMPs

In a stable gait, during the single support phase, the CoP of the supporting foot is also the ZMP of the whole exoskeleton; during the double support phase, the relationship between the ZMP and the CoP is described by

$$X_p = \frac{f_{LZ} X_L + f_{RZ} X_R}{f_{LZ} + f_{RZ}}, \quad Y_p = \frac{f_{LZ} Y_L + f_{RZ} Y_R}{f_{LZ} + f_{RZ}} \tag{17}$$

where

ZMP$= (X_p, Y_p, Z_p)$: ZMP of the whole biped
$\text{CoP}_L = (X_L, Y_L, Z_L)$: CoP of the left foot
$\text{CoP}_R = (X_R, Y_R, Z_R)$: CoP of the right foot
$f_L = (f_{LX}, f_{LY}, f_{LZ})$: ground reaction force at CoP_L
$f_R = (f_{RX}, f_{RY}, f_{RZ})$: ground reaction force at CoP_R.

To measure the ZMPs of the wearer and the exoskeleton, the foot-unit shown in Figure 5 was constructed. The wearer's foot rests on the upper plate, and the exoskeleton's leg is connected to the middle plate. There are four force sensors between the upper and middle plates, and four more between the middle and lower plates. The sensors are distributed as shown in Figure 6.

During the single support phase, sensors 1–4 measure the ground reaction force under the human foot, allowing the ZMP coordinates of the human in the foot's local coordinate frame to be obtained from

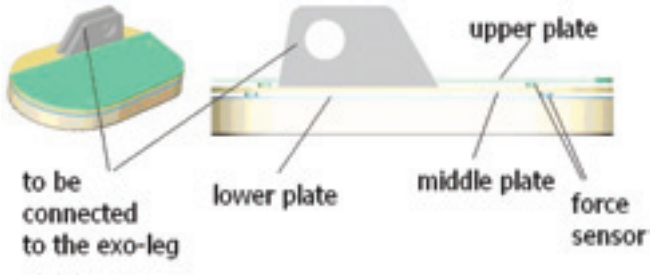

Figure 5. Design of the exoskeleton's foot unit.

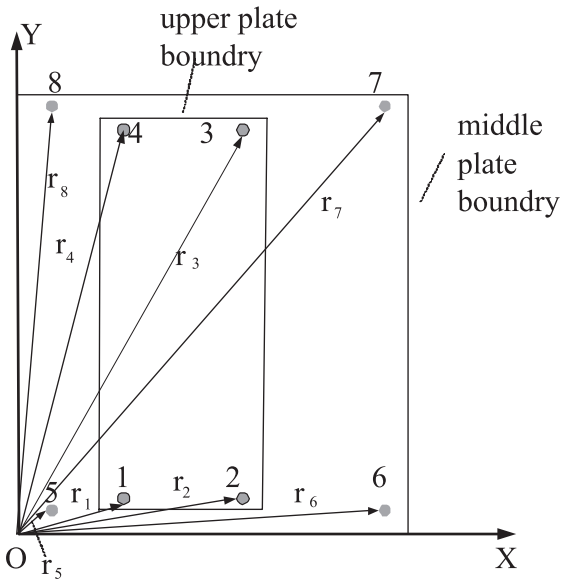

Figure 6. Location of the force sensors.

$$ZMP_h = \frac{\sum_{i=1}^{4} F_i r_i}{\sum_{i=1}^{4} F_i} \tag{18}$$

where F_i is the force measured by sensor i at the distance (r_i) from O, as defined in Figure 6. Sensors 5-8 measure the ground reaction force under the whole system (the human plus the exoskeleton). Similarly to the human's ZMP, the ZMP of the whole system can be calculated from

$$ZMP_w = \frac{\sum_{i=5}^{8} F_i r_i}{\sum_{i=5}^{8} F_i}. \tag{19}$$

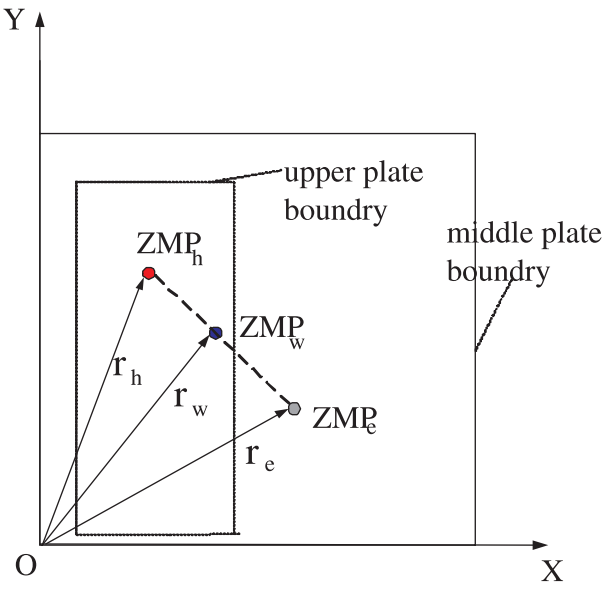

Figure 7. Relationship between the human's ZMP and the exoskeleton's ZMP.

The ZMP of the exoskeleton is on the straight line from the human's ZMP to the whole system's ZMP, and its position can be obtained from

$$ZMP_e = \frac{\sum_{i=1}^{4} F_i(r_w - r_h)}{\sum_{i=5}^{8} F_i - \sum_{i=1}^{4} F_i} + r_w \tag{20}$$

as we take the moment about the point ZMP_w,

$$\left(\sum_{i=5}^{8} F_i - \sum_{i=1}^{4} F_i\right)(ZMP_e - r_w) = \sum_{i=1}^{4} F_i(r_w - r_h) \tag{21}$$

in which r_h and r_w are the coordinates of the human's ZMP and the ZMP of the whole system (human plus exoskeleton), respectively, as shown in Figure 7. Note that the position of the ZMP is expressed in terms of X and Y coordinates.

During the double support phase, instead of the ZMPs, the CoPs of each foot are obtained from equations (18) to (20). By substituting those CoPs of the human and the exoskeleton into equation (17), the ZMPs of the human and the exoskeleton can be obtained.

3.4. Trunk Compensation

If the actual (measured) ZMP of the exoskeleton differs from the desired ZMP, trunk compensation is applied to shift the actual ZMP to an appropriate position.

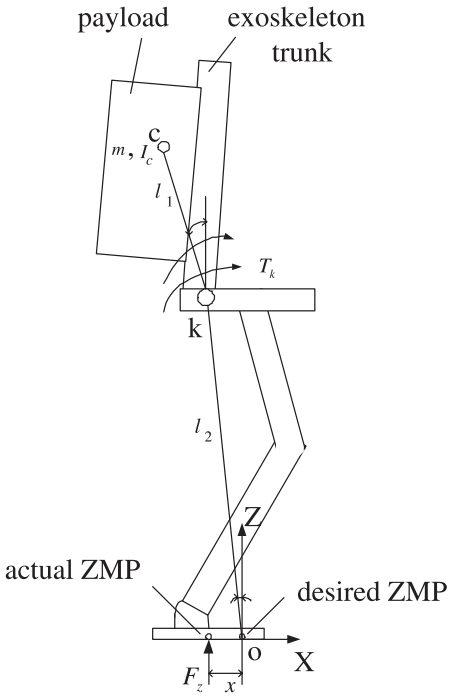

Figure 8. Adjusting the ZMP using trunk compensation.

Without losing generality, only motion in the sagittal plane during the single support phase is discussed here; trunk compensation in the frontal plane or during the double support phase is performed in the similar way.

As shown in Figure 8, the actual ZMP differs from the desired ZMP in the direction of X axis by Δx. Note that the ground reaction force F_z acting on the exoskeleton can be derived from $F_z = \sum_{i=5}^{8} F_i - \sum_{i=1}^{4} F_i$. For simplicity, we assume that the action of the trunk joint k will not cause a change in the motion at any other joint. The system will then behave as if it was composed of two rigid links connected at trunk joint k, as depicted in Figure 8. The payload and the exoskeleton trunk as shown in the figure are considered as an upper part of total mass m and inertia moment I_k around the axis of joint k (as $I_k = I_c + ml_1{}^2$). Point c is the center of mass of the upper part, and the distance from k to C is l_1. The lower part, representing the sum of all the links below the trunk joint k, including another leg that is not drawn in the figure, is also considered as a rigid body, which is standing on the ground surface and does not move; the distance from O to k is l_2. Note that ΔT_k stands for the correctional actuator torque, applied at joint k. It is assumed that the additional torque ΔT_k will cause a change in acceleration of the upper part $\Delta\ddot{\beta}$, but that velocities will not change due to the action of ΔT_k, $\Delta\dot{\beta} \approx 0$. Next, the following equations are derived:

$$\Delta T_k = I_k \Delta\ddot{\beta} \tag{22}$$

$$F_z \Delta x = \Delta T_k + ml_1 l_2(\cos\beta\cos\alpha + \sin\beta\sin\alpha)\Delta\ddot{\beta}. \tag{23}$$

From equation (22), we have

$$\Delta\ddot{\beta} = \frac{\Delta T_k}{I_k}. \tag{24}$$

Substituting equation (24) into equation (23), we obtain

$$\Delta T_k = \frac{F_z \Delta x}{1 + \dfrac{ml_1 l_2(\cos\beta\cos\alpha + \sin\beta\sin\alpha)}{I_k}}. \tag{25}$$

Taking into account the fact that ΔT_k is derived by introducing certain simplifications, an additional feedback gain K_{zmp} is introduced into equation (25) as

$$\Delta T_k = K_{zmp}\frac{F_z \Delta x}{1 + \dfrac{ml_1 l_2(\cos\beta\cos\alpha + \sin\beta\sin\alpha)}{I_k}} \tag{26}$$

where K_{zmp} can be determined from the feedback during actual walking. Equation (26) shows how to drive the actual ZMP towards the desired ZMP by controlling the torque output of the trunk joint.

4. CONTROL IMPLEMENTATION OF THE INTEGRATED EXOSKELETON

The important function of the inner exoskeleton is to read the required input data from the operator. This data will be analyzed, transformed into the corresponding command signals for the outer exoskeleton using certain mapping algorithms, and then transferred to the outer exoskeleton.

4.1. Real-Time Operating System

For the present work, xPC Target toolbox in MATLAB was employed as a real-time operating system for implementation of the controls. xPC Target provides a host-target prototyping environment that enables users to connect system simulation models (which can be created using the Simulink and Stateflow toolboxes from MATLAB) to physical systems and execute them in real time, and also provides comprehensive software capabilities for rapid prototyping and hardware-in-the-loop simulation of control and signal processing systems.

The xPC Target system runs on both the host PC and target PC, as shown in Figure 9. The host PC runs Microsoft Windows 2000 operating system and the required software packages: MATLAB, Simulink, Real-Time Workshop (RTW), xPC Target, and a C/C++ compiler; MATLAB is the host software environment for Simulink, RTW, and xPC Target. The command-line interface can be used to control and interact with the xPC Target software environment and target application. Simulink is used to model dynamic physical systems (ex-

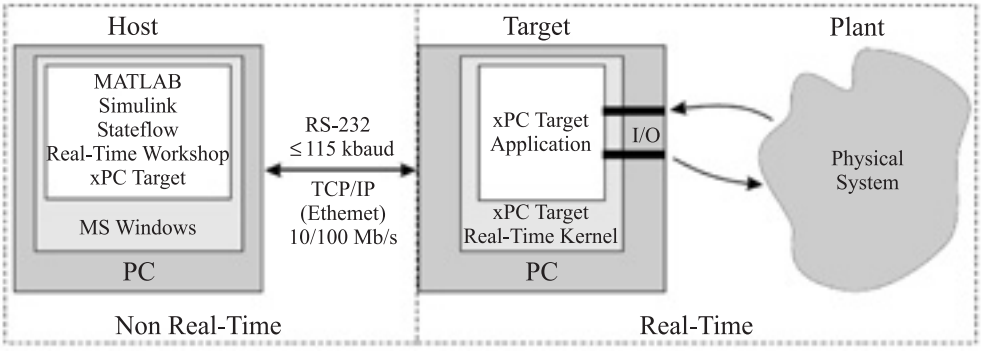

Figure 9. xPC Target system (adapted from Mosterman et al., 2005).

oskeleton systems in our work) and controllers using block diagrams. RTW and the C/C++ compiler convert Simulink blocks into C code and build a target application, which is then downloaded to the target PC and executed in real-time. Communication between the host PC and the target PC is through RS-232 since this is inexpensive and easy to use. The target PC runs the highly optimized xPC Target kernel, loaded from the boot disk. The kernel initiates host-target communication, activates the application loader, and waits for the target application to be downloaded from the host PC. The executable code generated on the host PC then runs in real-time on the target PC.

The I/O board is an adapted Sensoray model 626 card; when the executable code is running on the xPC target kernel, the required voltage signals are generated in the I/O board D/A channels according to the sensor readings and the controller designed using the Simulink blocks.

The voltage signals from the I/O board flow into power amplifiers as the reference signals. Proper output variables (voltage, current, etc.) from the amplifiers are then generated and used to drive the motors. The encoders are connected to the encoder channels of the I/O board, which read the encoder data into the program being executed on the target PC. New voltage reference signals from the I/O board are then generated based on the encoder readings. The overall architecture of the host-target hardware-in-the-loop exoskeleton control system established in this work is shown in Figure 10. Figure 11 shows the control system of the integrated exoskeleton.

4.2. Real-time Control of the LEE

The control structure most often applied on bipedal robots has four levels (Vukobratović et al., 1990), as shown in Figure 12:

1. highest control level
2. strategic control level
3. tactical control level
4. executive control level.

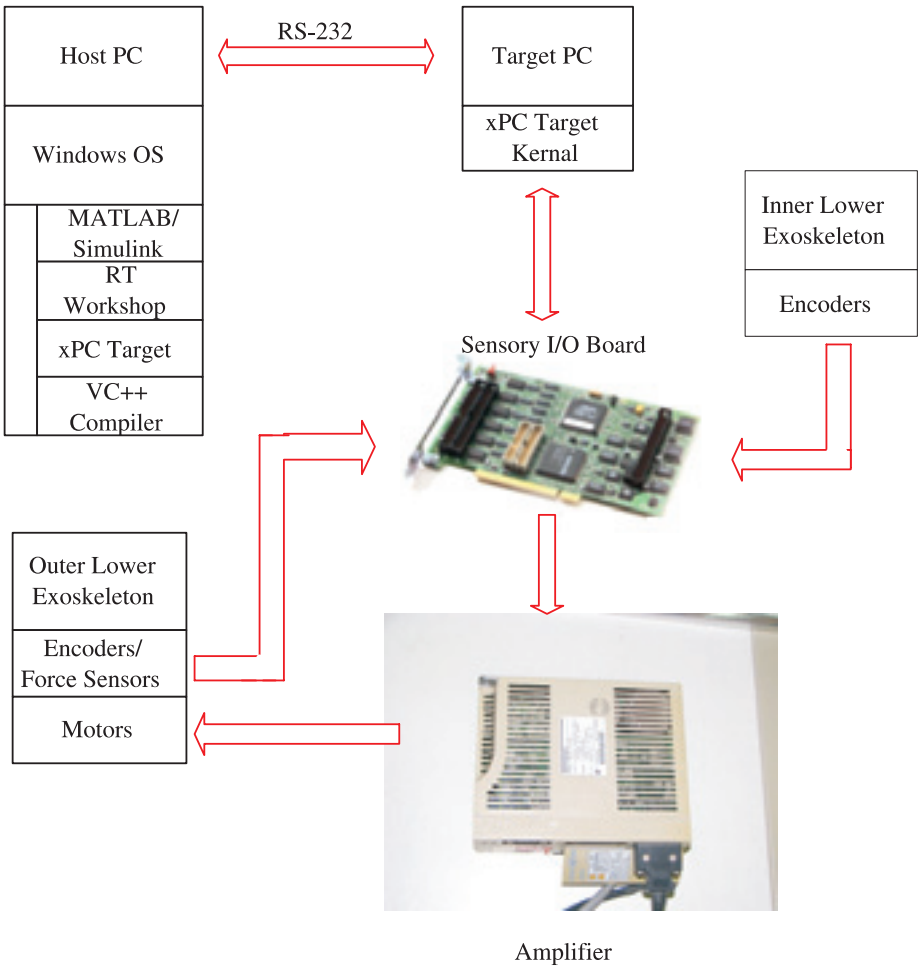

Figure 10. Control system architecture of the exoskeleton system.

The two upper control levels are generally recognized as the "intelligence" levels. Robots with the two upper levels such as ASIMO (http://www.hnoda.co.uk/ASIMO; Hirose et al., 2001), QRIO (http://www.sony.net/SonyInfo/QRIO/story/index_nf.html), HRP-2 (Kanehiro et al., 2003; Kaneko et al., 2004), etc. able to walk across terrain of unknown profile. Robots walking in a known environment, where the trajectory of each link can be pre-defined offline, do not need the two upper levels. The tactical level generates the trajectory required from each degree of freedom (DoF) in order to achieve the desired overall functional movement. Lastly, the executive level executes these trajectories by means of the appropriate actuators.

Instead of artificial intelligence, the highest level of the exoskeleton's control structure is implemented through the human user. The user recognizes the obstacles using his or her natural sensory systems, and decides where to go and how to get that. The second level is the transfer of human intention to the exoskeleton's controller and the controller's division of the

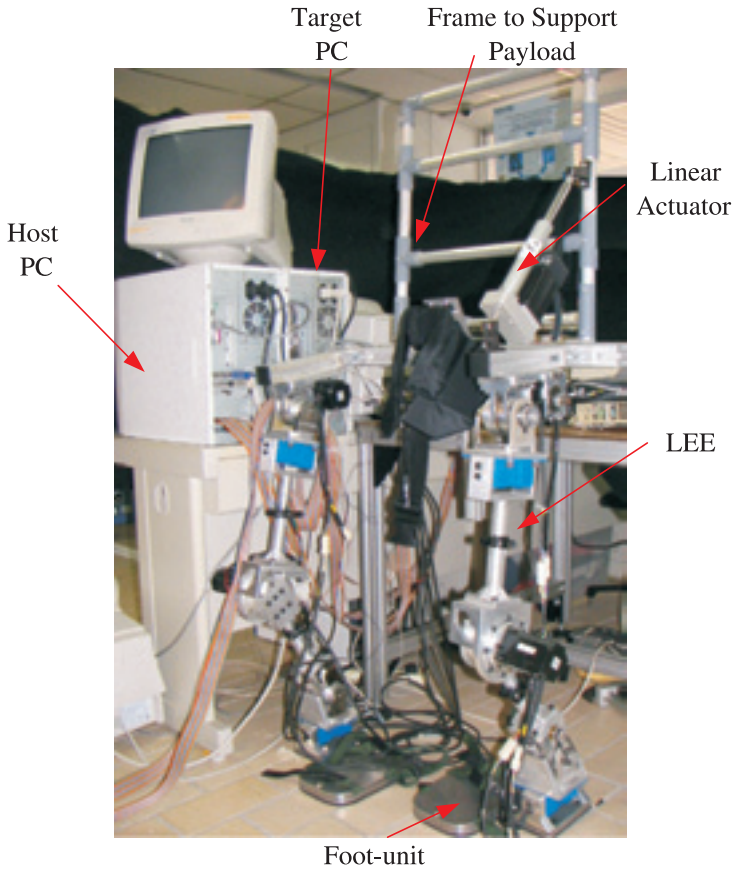

Figure 11. The control system and full experimental set-up for the integrated exoskeleton.

required operation into elementary movements. The two lowest control levels are similar to those of robots, and the exoskeleton can be seen, for these, as a robot with human intelligence integrated.

4.2.1. Control of the Inner/Outer Exoskeleton Joints

In this section, the two lowest control levels are tested to check whether the joints of the exoskeleton can perform the desired trajectories in real time. Two I/O boards are employed in this work; each board reads six the encoders and controls the three motors of one leg. Channels 1 (hip), 2 (knee), and 3 (ankle) read the counts from the encoders of the inner exoskeleton, while channels 4 (hip), 5 (knee), and 6 (ankle) read the counts from the encoders of the outer exoskeleton. The counts are then converted into degrees and compared. The difference between the inner and outer exoskeletons' corresponding joints is converted to a command signal through the PID controller. A suitable voltage is then applied to the amplifiers and motors to drive the LEE to match the joint motion of the inner exoskeleton.

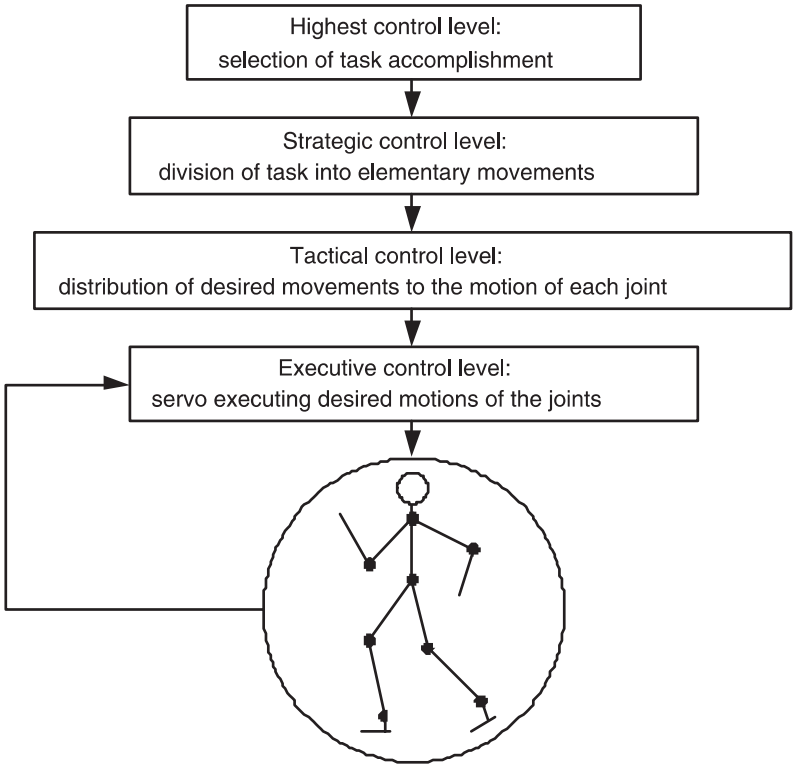

Figure 12. Hierarchical architecture of control biped locomotion (from Vukobratović et al, 1990).

Figure 13 shows the response of LEE's left knee joint during one sample test. The two upper curves representing the inner exoskeleton and the LEE (outer exoskeleton) are quite close to each other, while the lower line represents the difference between the inner exoskeleton and the LEE. Figure 14 shows the difference at an enlarged scale.

We experimentally applied the exoskeleton control scheme during the rehabilitation process of a clinical trial with a patient whose left leg had become weak after strokes; Figure 15 shows a series of snapshots. The patient found that the exoskeleton's leg responded well and he could hardly feel any extra burden.

4.3. Control of the Exoskeleton and Walking Experiments

4.3.1. Walking Test with the ZMP control

The path for the walking test is illustrated in Figure 16. First, the human stands up, with a separation of 300 mm between his left and right feet. He then walks forward, beginning by moving his right foot, from position R1 to R2. Next, his left foot moves from position L1 to position L2; his right foot then moves again, from position R2 to position R3. Finally, his left foot moves from position L2 to position L3 and he returns to the standing posture. Note that the step length is 300 mm. The reading from each of the four force sensors below

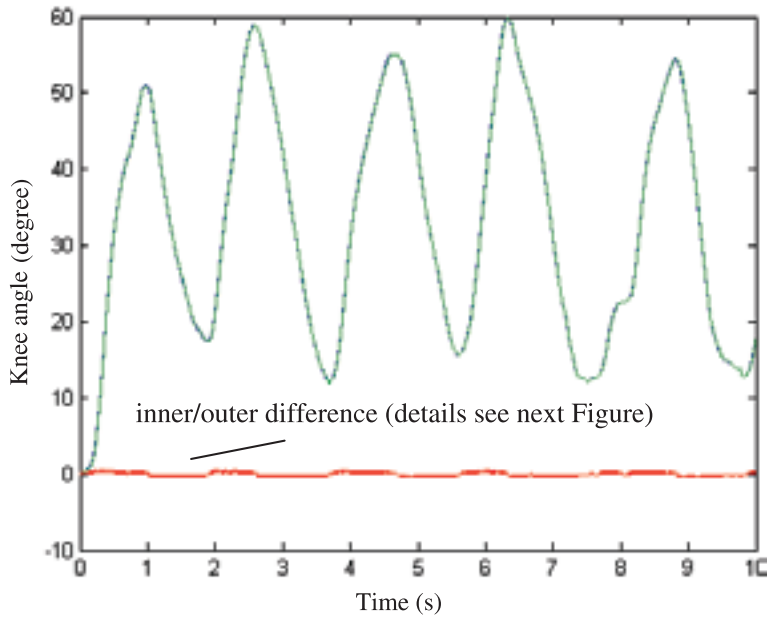

Figure 13. Response of the left knee joint.

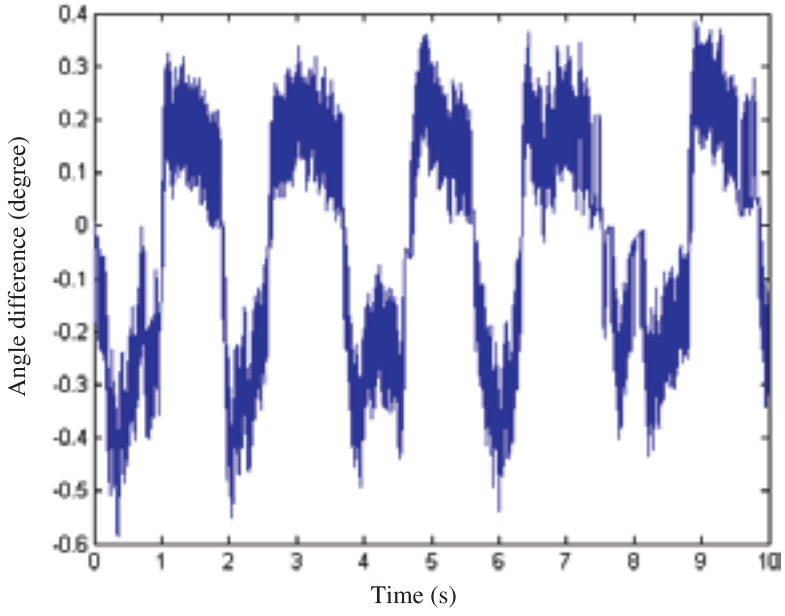

Figure 14. Angular difference between the inner exoskeleton and the LEE and telephony.

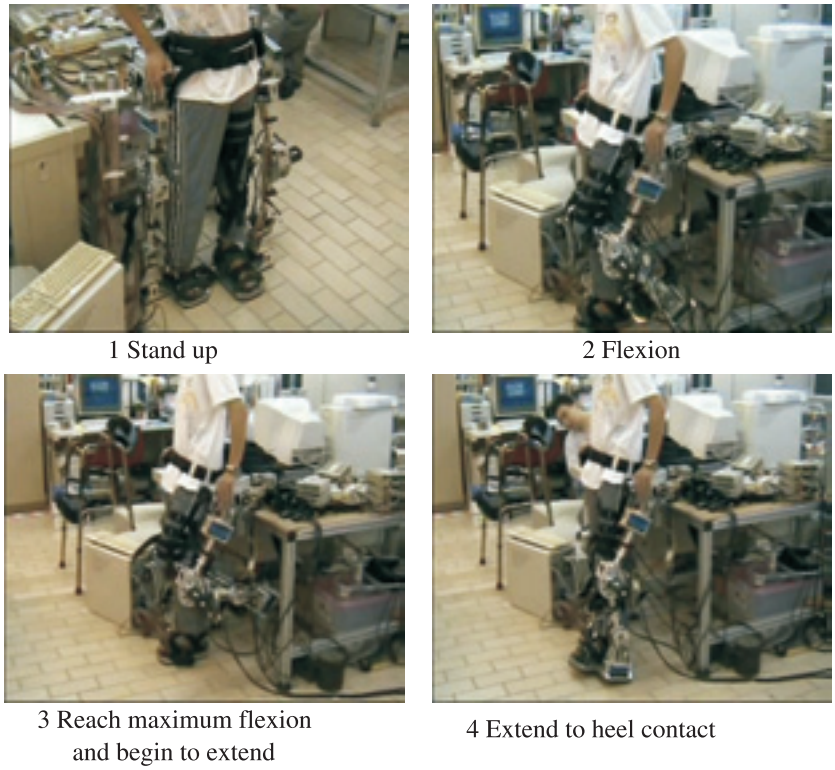

Figure 15. Exoskeleton trial with a post-stroke patient.

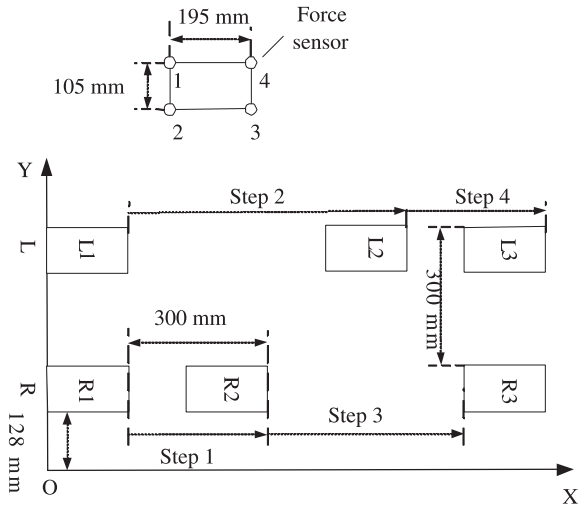

Figure 16. Steps of the walking experiment, conducted with Sensors 1 to 4 below the human's foot.

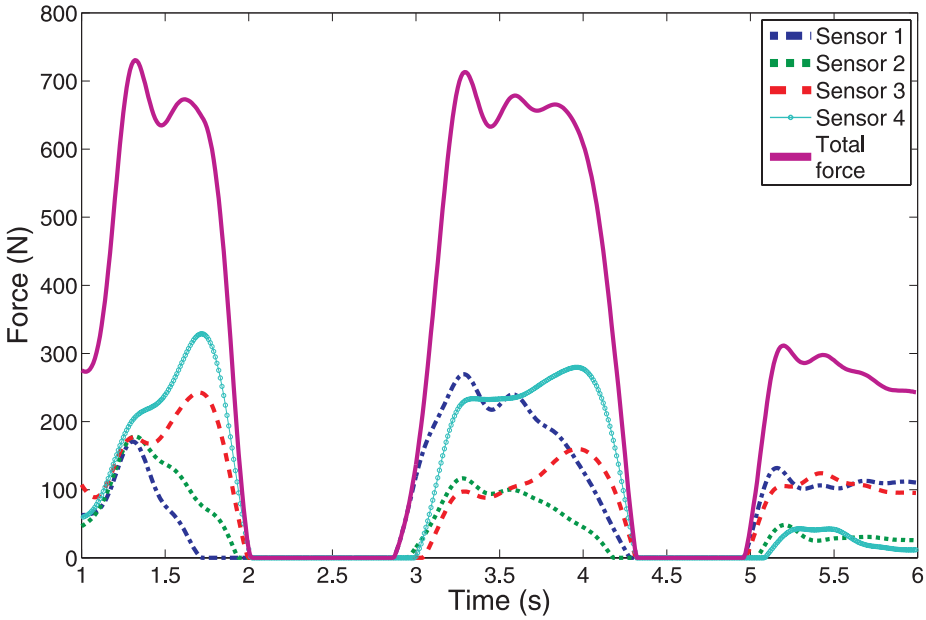

Figure 17. Ground reaction force below the left foot.

each foot, and the total force, are shown in Figures 17 and 18, for the left foot and right foot respectively. Figure 19 shows the timing of the ground reaction force below the two feet, with the ends of the horizontal axis marking the points where the system leaves, and returns to, the standing posture.

The ZMP of the human can be evaluated (see Figure 20) by making use of equations (17) and (18). Note that the XY coordinates in this section are different from those defined in Figures 6 and 7, for convenience of illustration. Figures 19 and 20 show that when the person begins to walk, the ground reaction force below his right foot decreases, while the force below his left foot increases. The ZMP shifts from between the two feet to the left foot, i.e., the supporting area. During the walk, the ZMP shifts between the two feet. Finally, when the human returns to the standing posture, the ZMP moves back to its original position between the two feet.

4.3.2. Incorporation with the online Balancer

An online balancer is employed in the control scheme, as shown in Figure 21. The balancer module reads the current joint angles and measured human ZMP, and the exoskeleton's desired ZMP is then calculated. If the exoskeleton's measured ZMP differs from the desired one, a suitable command signal will be applied to the actuator of the trunk joint, and the trunk will then move to shift the actual ZMP toward the desired position, as described in Section 3.

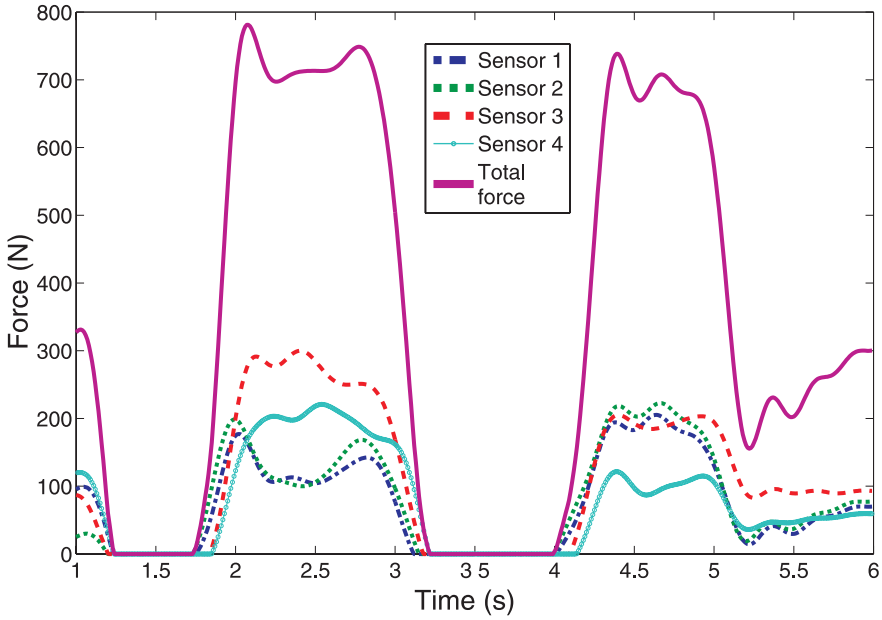

Figure 18. Ground reaction force below the right foot.

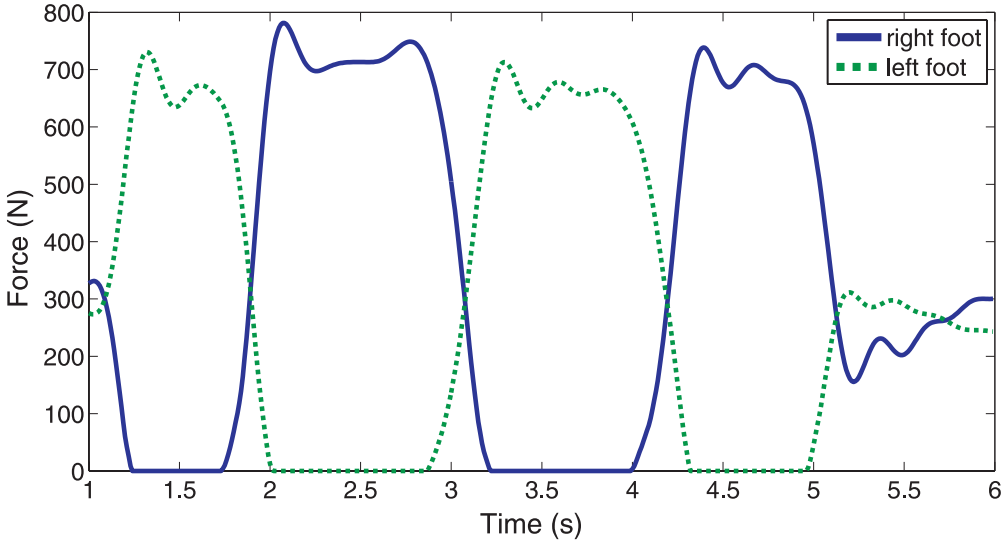

Figure 19. Changes in the ground reaction forces below the two feet with time.

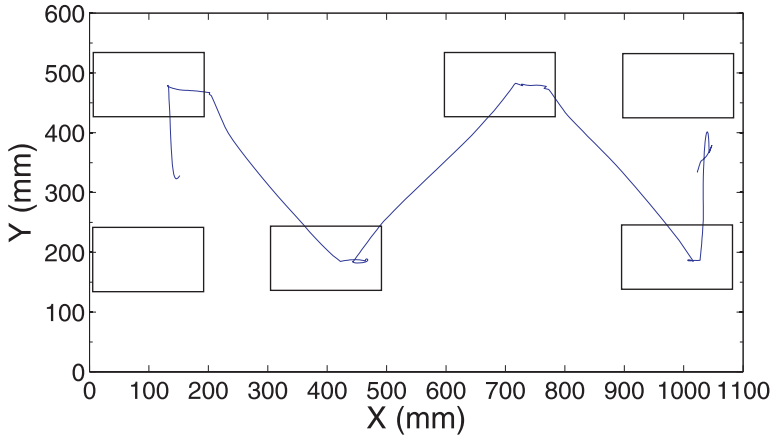

Figure 20. ZMP trajectory in the XY coordinate system.

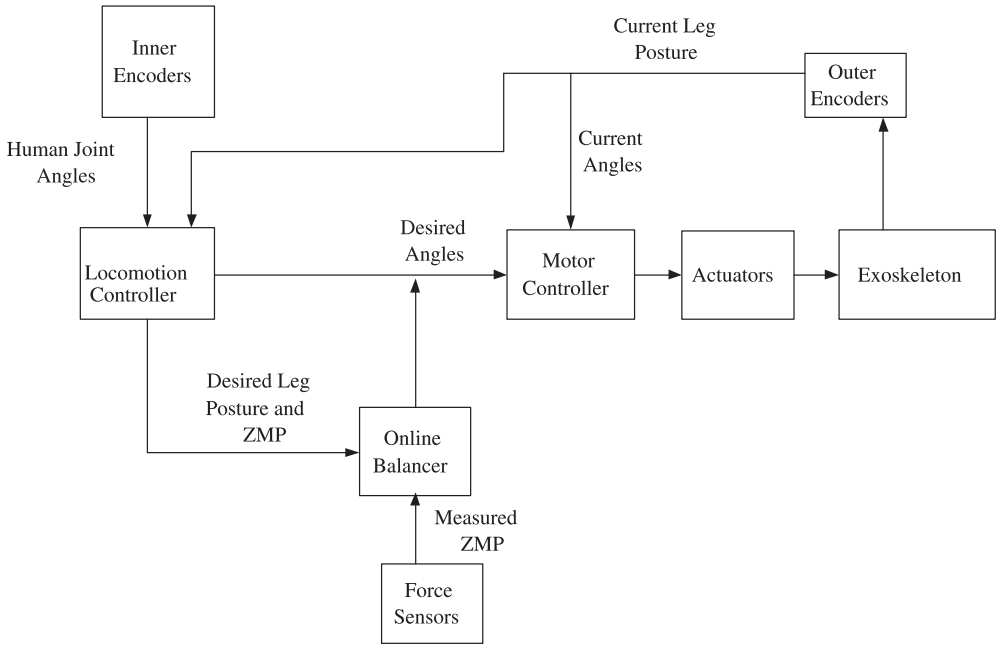

Figure 21. Signal flow diagram.

A walking experiment was performed to check the balancer module, using a walk procedure similar to that in Figure 16. Figure 22 shows the trajectories of the human and exoskeletal ZMPs in the XY coordinate system, demonstrating that the ZMP is adjusted during the single support phase to ensure that it is always kept inside the support area. Hence, the exoskeleton can walk stably with the user. To illustrate the relationship between the human and exoskeletal ZMPs more clearly, Figures 23 and 24 show the X and Y coordinates (respec-

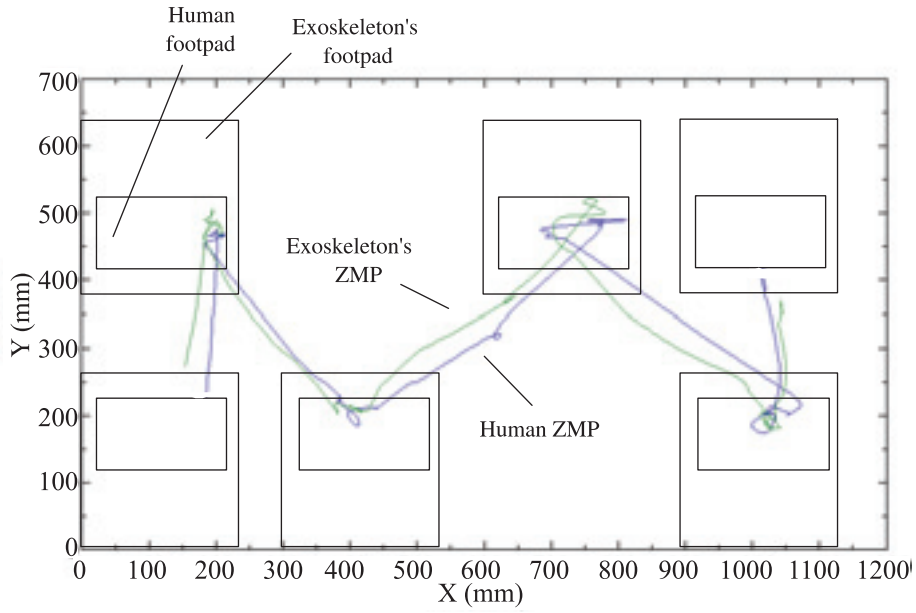

Figure 22. Human and exoskeletal ZMP trajectories in the XY coordinate system.

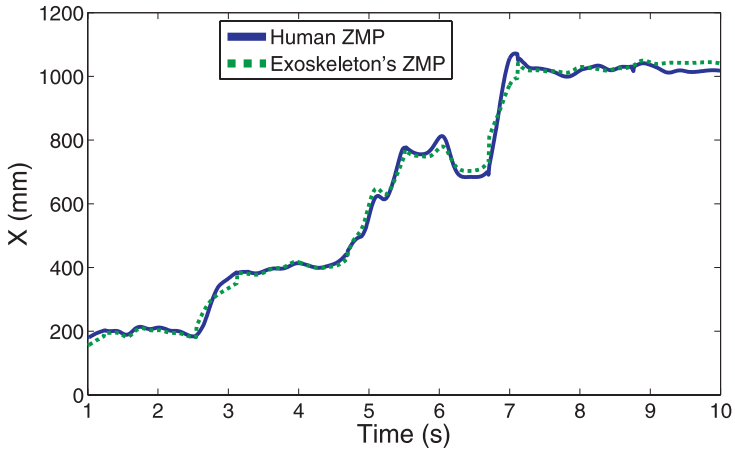

Figure 23. X coordinate of the human and exoskeletal ZMPs with respect to time.

tively) of the human and exoskeleton ZMPs with respect to time, by virtue of the equations derived in Section 3.3. Note that the relations between ZMP_e, ZMP_h, and ZMP_w have been illustrated in Figure 7. The ZMP of the exoskeleton (ZMP_e) is obtained by virtue of equation (20). These results in Figures 23 and 24 show that in the X direction, the exoskeleton's ZMP is close to the human ZMP due to the trunk compensation, which ensures that the exoskeleton can walk stably while following the human. In the Y direction, the difference

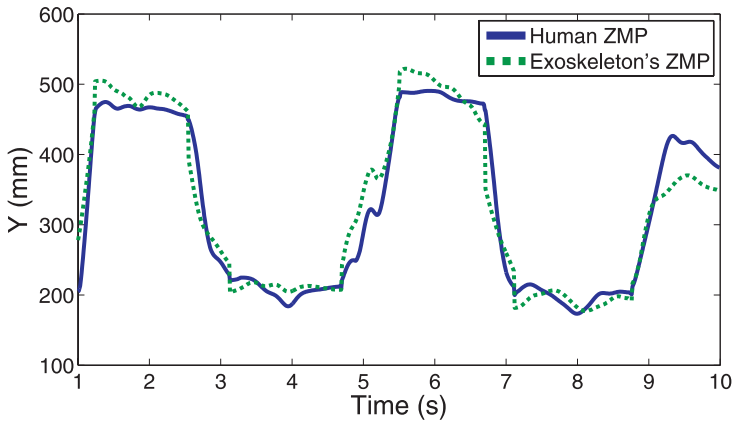

Figure 24. Y coordinate of the human and exoskeletal ZMPs with respect to time.

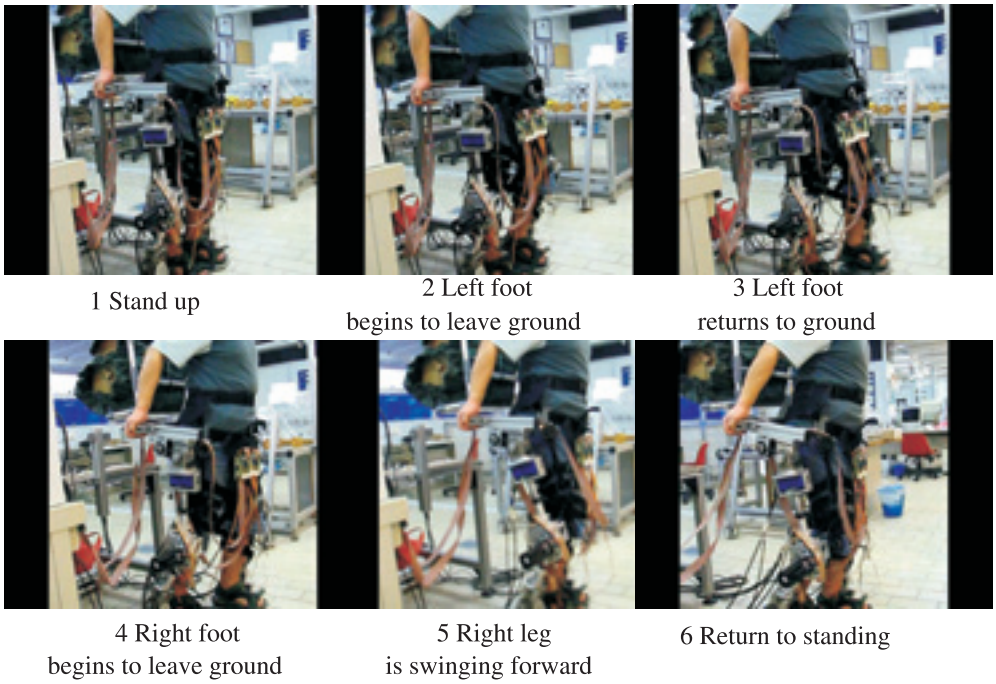

Figure 25. Snapshots of a walking test.

between exoskeleton's ZMP and the human ZMP is larger. This is because the exoskeleton's foot-unit is much wider than the human foot within it (see Figures 6, 22 and 24), and the allowable range of the exoskeleton's ZMP in Y direction is therefore larger.

More experiments were performed including walking forward and backward. Figure 25 shows some snapshots of one of these experiments.

5. CONCLUSIONS

This article has presented a wearable lower exoskeleton system developed for enhancement of human walking ability, which incorporates a human as an integral part of the control system. The methodology used in designing an anthropomorphic and adaptable exoskeleton system has been discussed. Real-time locomotion control of the integrated exoskeleton has been implemented. Several walking experiments using the ZMP control were conducted, and some experimental results have been presented in this article. Future work should focus on designing a more compact and comfortable exoskeleton constructed from lighter materials and allowing more degrees of freedom. The control algorithm can be improved to be more robust and adaptable to various conditions. For practical application, the system should have a seamless on-board embedded system. An untethered, portable, and mountable power generation subsystem remains a more challenging issue for future applications.

Acknowledgements. The authors would like to thank the reviewers for their constructive comments, which helped to improve the quality of the article. Thanks are also due to Miss Yunyun Huang, Mr. Tien-Boon Tan, Mr. Sui-Nan Lim, Mr. Tze-Kuang Ng and Mr. Rene Wachter for their assistance in programming and conducting experiments. This research is supported by the Research Grant MINDEF-NTU/02/01 from the Ministry of Defence, Singapore. The Robotics Research Center of the Nanyang Technological University provided technical help, as well as space and facilities. The MATLAB and xPC Target software, provided by TechSource Systems Pte. Ltd., is also appreciated.

REFERENCES

Kasaoka, K. and Sankai, Y., 2001, "Predictive control estimating operator's intention for stepping-up motion by exoskeleton type power assist system HAL," in *Proceedings of the IEEE/RSJ International Conference on Intelligent Robots and Systems*, pp. 1578–1583.

Kawamoto, H. and Sankai, Y., 2002, "Comfortable power assist control method for walking aid by HAL-3," in *Proceedings of IEEE International Conference on Systems, Man and Cybernetics* **4**, 6 pages.

Kawai, S., Naruse, K., Yokoi, H., and Kakazu, Y., 2004, "A study for control of a wearable power assist system-recognition of human motions by surface EMG signals," in *Proceedings of the 2004 IEEE/RSJ International Conference on Intelligent Robots and Systems (IROS2004)*, pp. 1–6.

Naruse, K., Kawai, S., Yokoi, H., and Kakazu, Y., 2003a, "Development of wearable exoskeleton power assist system for lower back support," in *Proceedings of the 2003 IEEE/RSJ International Conference on Intelligent Robots and Systems (IROS2003)* (CD-ROM).

Naruse, K., Kawai, S., Yokoi, H., and Kakazu, Y., 2003b, "Design of compact and lightweight wearable power assist device," in 2003 *ASME International Mechanical Engineering Congress and Exposition*, Washington, DC, November 16–21.

Berkeley Exoskeleton, Berkeley Robotics Laboratory, http://bleex.me.berkeley.edu/bleex.htm.

Liu, X., Low, K. H., and Yu, H. Y., 2004, "Development of a lower extremity exoskeleton for human performance enhancement," in *Proceedings of the 2004 IEEE/RSJ International Conference on Intelligent Robots and Systems*, pp. 3889–3894.

Liu, X. and Low, K. H., 2004, "Development and preliminary study of the NTU lower extremity exoskeleton," in *Proceedings of 2004 IEEE Conference on Cybernetics and Intelligent Systems (CIS 04)*, pp. 1242–1246.

Low, K. H., Liu, X., Yu, H. Y., and Kasim, H. S., 2004, "Development of a lower extremity exoskeleton – preliminary study for dynamic walking," in *Proceedings of the Eighth International Conference on Control, Automation, Robotics and Vision*, pp. 2088–2093.

Whittle, M. W., 1991, *Gait Analysis: An Introduction*, Butterworth-Heinemann, Oxford, UK.

Vukobratović, M. and Juricic, D., 1969, "Contribution to the synthesis of biped gait," *IEEE Transactions on Bio-Medical Engineering* **16(1)**, 1–6.

Vukobratović, M., Borovać, B., Šurdilović, D., and Stokić, D., 2001, "Humanoid robots," in *The Mechanical Systems Design Handbook: Modeling, Measurement, and Control*, Hurmuzlu, Y. and Nwokah, O. D. I., eds., Southern Methodist University, Dallas, TX.

Marchese, S., Muscato, G., and Virk, G. S., 2001, "Dynamically stable trajectory synthesis for a biped robot during the single-support phase," in *Proceedings of IEEE/ASME International Conference on Advanced Intelligent Mechatronics*, Vol. 2, pp. 953–958.

Mosterman, P., Prabhu, S., Dowd, A., Glass, J., Erkkinen, T., Kluza, J., and Shenoy, R., 2005 "Embedded real-time control via MATLAB, Simulink, and xPC Target," in *Handbook on Networked and Embedded Systems*, Birkhauser, Boston, MA.

Vukobratović, M., Borovac, B., Surla, D., and Stokić, D., 1990, *Biped Locomotion: Dynamics, Stability, Control, and Application,* Springer-Verlag, Berlin.

ASIMO, The Humanoid Robot by Honda, http://www.honda.co.jp/ASIMO.

Hirose, M., Haikawa, Y., Takenaka, T., and Hirai, K., 2001, "Development of humanoid robot ASIMO," in *IEEE/RSJ International Conference on Intelligent Robots and Systems – Workshop 2*, Maui, HI.

QRIO, The Humanoid Entertainment Robot by SONY, http://www.sony.net/SonyInfo/QRIO/story/index_nf.html.

Kanehiro, F., Kaneko, K., Fujiwara, K., Harada, K., Kajita, S., Yokoi, K., Hirukawa, H., Akachi, K., and Isozumi, T., 2003, "The first humanoid robot that has the same size as a human and that can lie down and get up," in *Proceedings of the 2003 IEEE International Conference on Robotics and Automation*, pp. 1633–1639.

Kaneko, K., Kanehiro, F., Kajita, S., Hirukawa, H., Kawasaki, T., Hirata, M., Akachi, K., and Isozumi, T., 2004 "Humanoid robot HRP-2," in *Proceedings of the 2004 IEEE International Conference on Robotics and Automation*, pp. 1083–1090.